AD-A145 297 A NONLINEAR THEORY FOR GYRO-DEVICES(U) VARIAN BEVERLY 1/1
MICROWAVE DIV MA G E THOMAS 1984 N00014-82-C-2192

UNCLASSIFIED F/G 12/1 NL

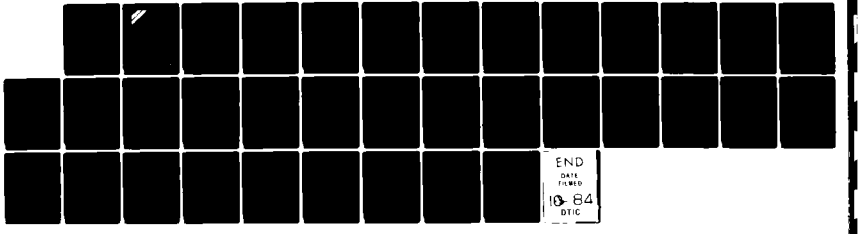

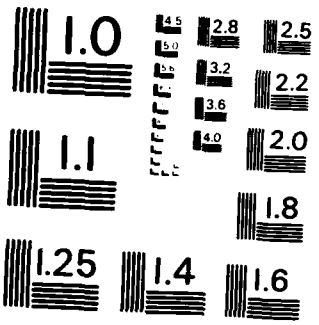

(2)

AD-A145 297

A NONLINEAR THEORY FOR GYRO-DEVICES

FINAL REPORT

CONTRACT NO. N00014-82-C-2192

varian

GR

A NONLINEAR THEORY FOR GYRO-DEVICES

FINAL REPORT

CONTRACT NO. N00014-82-C-2192

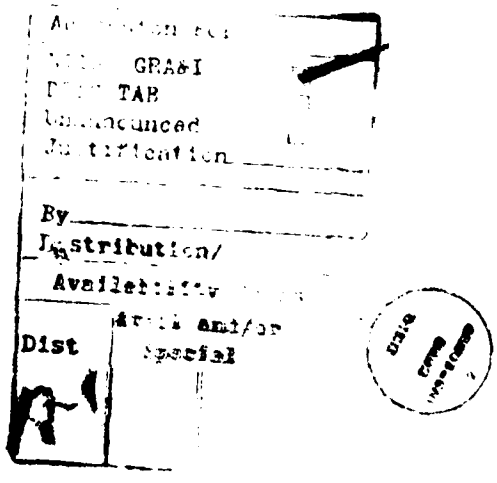

A NONLINEAR THEORY FOR GYRO-DEVICES

G. E. THOMAS

VARIAN ASSOCIATES, INC.

EIGHT SALEM ROAD

BEVERLY, MA 01915

ABSTRACT

Recent work on a nonlinear theory for gyro-devices (i.e., gyrotrons, gyro-twts, gyro-klystrons) is described. Differences between this work and similar work (Thomas, 1981) are emphasized. Comparisons are made between theoretical predictions and computer simulations. In addition, comparisons are made between theoretical predictions and 60 GHz gyrotron experimental data.

A NONLINEAR THEORY FOR GYRO-DEVICES

G. E. THOMAS

VARIAN ASSOCIATES, INC.

1.0 INTRODUCTION

With the increasing need for both higher power/higher frequency gyrotrons and for radar quality gyro-twts and gyro-klystrons, it is important that a more complete understanding of the basic gyro-device interaction be obtained. It is no longer sufficient just to predict power and efficiency. Other effects such as harmonic generation, phase stability, etc., must be well understood and predictable. To accomplish the task of modeling such nonlinear effects, a nonlinear theory (Thomas 1981, 1983) is used. Before work can begin on predicting general behavior resulting from nonlinear effects, it is important that predictions of the nonlinear theory show close agreement with computer simulations and experiments. The nonlinear theory has been extended to the point where there is close agreement between theoretical predictions and work (computer simulation and experimental) done at Varian/Palo Alto.

In this paper, the recent theoretical work based on the concept of the soliton is described in detail (SECTION 2.0). Differences between the previous nonlinear work and this recent work are discussed. These differences are as follows;

1) The inclusion of the effect of the rf fields on the electron equations of motion.

2) The inclusion of higher cyclotron harmonics in the higher order dispersive terms.

3) A more complete equation for the number density.

4) The inclusion of dispersive effects in the direction of fast wave propagation.

5) The inclusion of the effects of the rf field on the operating range of the gyro-device.

By including these changes, one has not only derived a nonlinear partial differential equation which describes the dynamic evolution of the nonlinear interaction between the rf fields and the electron plasma in a gyro-device, but from an understanding of this equation, one can determine and predict the saturation mechanism which limits the device's operating range. This saturation mechanism is discussed in Section 3.0. In Section 4.0 theoretical predictions of the magnetic field where saturation begins and the peak rf output power of a given gyro-device design are compared to available simulation results and experimental data. Conclusions and areas for future work are given in Section 5.0.

2.0 THE NONLINEAR THEORY

The general technique used to derive the nonlinear partial differential equation describing the rf field-electron plasma interaction in a gyro-device consist of the following steps:

1) The derivation of a partial differential equation. This equation is derived using the method of characteristics (Krall and Trivelpiece, 1973,) where the effect of the rf electric field on the motion of the electrons is included in zero order.

2) The derivation of a number density equation describing the effect of the rf electric field on the electron beam. This equation includes the effect of the dominant nonlinearity which is also responsible for electron bunching.

3) The partial differential equation and the number density equation are coupled together and result in a nonlinear partial differential equation.

4) The nonlinear partial differential equation is reduced by a multiple time scales perturbation technique such that at second order (i.e., slowly varying) a modified nonlinear Schrodinger equation (MNLSE) is obtained.

5) The terms of the MNLSE are ordered such that if the coefficients have the proper signs, the two dimensional cubic nonlinear Schrodinger equation (NLSE) is obtained at zero order.

6) The effects of the terms that modify the nonlinear equation from the two dimensional NLSE to the MNLSE are determined. Typically, additional dispersive terms result in growth or damping.

7) The region in parameter space in which one obtains growing soliton-like solutions is determined.

In this paper, each of these steps is decribed in sufficient detail to make the general technique clear. When possible, reference is made to previous work, therefore, only the most recent results are discussed.

2.1 DERIVATION OF THE PARTIAL DIFFERENTIAL EQUATION

The general technique for deriving the partial differential equation for gyro-devices is well known (CHU, et. al., 1979). The Vlasov-Maxwell equation is solved for a perturbed electron distribution function using the method of characteristics. For gyro-devices, the assumed electron distribution function is typically a delta function in both parallel and perpendicular velocity (i.e., $f_o=(\delta(P_\parallel)\delta(P_\perp - P_o)/2\pi P_\perp)$). In previous work, the electron equations of motion only included the effect of dc fields. However, wave propagation through an electron plasma can be significantly different if the wave drastically alters the motion of the individual electrons. Therefore, the effect of the rf field on the electrons is included in the zero order equations of motion. Including the rf field in the electron motion is the first major difference between this nonlinear theory and the previous work.

Because bunched electrons have the greatest effect on rf wave propagation, these are the electrons of interest. The assumption is made that for bunched electrons the rf fields appear quasi-static. It should be noted that this assumption does not imply that there are any bunched electrons nor does this assumption indicate anything concerning the mechanism of electron bunching. The mechanism of electron bunching is modeled by the number density equation and is discussed later. The validity of this assumption is supported by the fact that the angular frequency of interest is no longer the fast time scale parameter, ω, but instead, is the slow time scale parameter $\omega-\Omega'$. With the geometry shown in Figure 1 and a transformation to the rotating frame of reference, the following set of equations is obtained;

$$v_x = -v_\perp \cos(\Theta-(\omega-\Omega')t)-E_y/B_o \tag{1a}$$

$$v_y = -v_\perp \sin(\Theta-(\omega-\Omega')t) \tag{1b}$$

$$v_z = v_\parallel \tag{1c}$$

where $\Omega'=\Omega/\gamma$. Notice that a non-time varying ExB drift is included in (1a).

Substituting the above set of equations into the Maxwell-Vlasov equation and integrating over velocity space, a series of terms are obtained which contain Bessel functions. These Bessel funcions are treated differently in the present nonlinear theory than in both previous linear and nonlinear theories. In linear theory (Chu, et. al., 1979) the Bessel functions are used to describe the rf field character of the various modes. In the previous nonlinear theory (Thomas, 1981), expansions of the Bessel functions for small arguments were taken to obtain higher order dispersive terms. These expansions assumed that the order of the Bessel functions remained at one, (i.e., N=1). N was chosen equal to

one because the assumption was made that the gyro-device interaction is a resonant interaction at $\omega=\Omega$, and therefore, any harmonic cyclotron interactions are negligible. This assumption is not valid if the interaction is strongly nonlinear such that higher order electron motion exists as a result of the interaction of the rf field with the electron plasma. Higher order electron motion is no longer described by simple motion about a magnetic field line, but rather, contains cycloiding components superimposed on the simple motion (Figure 2). This additional motion indicates that the electron plasma has become weakly turbulent and contributes to higher order dispersion. Therefore, Bessel function expansions with N=1, N=2, and N=3 are used:

$$N^2 J_N^2(\alpha) = (1/4)(1^2)\alpha^2 - (1/16)(2^2)\alpha^4 + (1/64)(3^2)\alpha^6 \qquad (2)$$

where N=1 contributes to k_x^0 terms, N=2 contributes to k_x^2 terms, and N=3 contributes to k_x^4 terms. The inclusion of these higher order cyclotron harmonic terms in the higher order dispersive terms is the second major difference between the previous nonlinear theory and the work presented here.

By substituting the above Bessel function expansions into the various component terms resulting from the integration of the Vlasov-Maxwell equation over velocity space, the following equation is obtained;

$$A\frac{\partial^2 E_y}{\partial x^2} + B\frac{\partial^4 E_y}{\partial x^4} + C\frac{\partial^2 E_y}{\partial z^2} + D\frac{\partial^2 E_y}{\partial t^2} = 0 \qquad (3)$$

where the coefficients are as follows;

$$A = -\left[1 + \frac{\omega_p^2}{2\gamma\Omega^2}\frac{v_\perp^2}{c^2}\left(\frac{3(\omega - \Omega/\gamma)}{\omega - (k_{\parallel}v_{\parallel} + 2\Omega)/\gamma - k_x E_y/B_o} - \frac{v_\perp^2}{\gamma^2 c^2}\frac{(\omega - \Omega/\gamma)(k_{\parallel}v_{\parallel} + 2\Omega)/\gamma}{(\omega - (k_{\parallel}v_{\parallel} + 2\Omega)/\gamma - k_x E_y/B_o)^2}\right)\right] \quad (4a)$$

$$B = -\frac{9\,\omega_p^2 v_\perp^4}{32\,\gamma\,\Omega^4 c^2}\left[\frac{5(\omega - \Omega/\gamma)}{\omega - (k_{\parallel}v_{\parallel} + 3\Omega)/\gamma - k_x E_y/B_o} - \frac{v_\perp^2}{\gamma^2 c^2}\frac{(\omega - \Omega/\gamma)(k_{\parallel}v_{\parallel} + 3\Omega)/\gamma}{(\omega - (k_{\parallel}v_{\parallel} + 3\Omega)/\gamma - k_x E_y/B_o)^2}\right] \quad (4b)$$

$$C = -\left(1 + \frac{\omega_p^2 v_\perp^2}{\gamma c^2}\frac{1}{(\omega - (k_{\parallel}v_{\parallel} + \Omega)/\gamma - k_x E_y/B_o)^2}\right) \quad (4c)$$

$$D = \left[1 - \frac{\omega_p^2}{\gamma\omega^2} - \frac{\omega_p^2 v_\perp^2}{2\gamma^3\omega^2 c^2}\frac{(k_{\parallel}v_{\parallel} + \Omega)/\gamma}{(\omega - (k_{\parallel}v_{\parallel} + \Omega)/\gamma - k_x E_y/B_o)}\right] \quad (4d)$$

As a result of including the rf electric field in the electron equations of motion, the rf electric field appears in the denominator of all four coefficients. As a result of including N=2(3), terms like $2\Omega(3\Omega)$ appear in the numerator and denominator of the A(B) coefficient.

2.2 DERIVATION OF THE NUMBER DENSITY EQUATION

The number density equation describes the effect of the wave on the electron plasma. In other words, the number density equation models the bunching of the electrons which is a result of the ponderomotive force. This ponderomotive force is not the usual ponderomotive force acting along the direction parallel to the dc magnetic field, but is the ponderomotive force acting in the direction of the rotating electrons resulting in bunching transverse to the direction of wave propagation. The previous nonlinear theory did not take into account electron motion in the $\hat{z}$ direction when considering the bunching mechanism. $\hat{Z}$ directed motion is considered in the more complete fluid number density equation given below;

$$\frac{\partial^2 n_1}{\partial t^2} - v_z^2 \frac{k_z^2}{k_x^2} \frac{\partial^2 n_1}{\partial x^2} = - \frac{\partial}{\partial x} \left(\frac{F_{NL}}{m}\right) \tag{5}$$

where v_z is the wave group velocity and n_1 is the perturbed number density. Assuming a plane wave solution and transforming into the rotating frame yields;

$$-(\omega - \Omega')^2 \, n_1 + v_z^2 \frac{k_z^2}{k_x^2} k_x^2 \, n_1 = - \frac{\partial}{\partial z} \left(\frac{F_{NL}}{m}\right) \tag{6}$$

By substituting the expression for the ponderomotive force into (6), the following expression is obtained for n_1;

$$n_1 = \frac{\omega_p^2 |E|^2 (\omega - \Omega')/\omega}{8\pi n_o \omega^2 m} \Bigg/ \left[\frac{(\omega - \Omega')^2}{k_x^2} - v_z^2 \frac{k_z^2}{k_x^2} \right] \tag{7}$$

2.3 DERIVATION OF THE FULL NONLINEAR PARTIAL DIFFERENTIAL EQUATION

The full nonlinear partial differential equation is obtained by combining the two coupled equations (3) and (5) into a single nonlinear equation. (3) is coupled to (5) because it contains n_1 in its coefficients in the form of ω_p^2. (5) is coupled to (3) because it has $|E|^2$ in the ponderomotive force term. Using (7) and $n=n_o+n_1$, the following is obtained;

$$A^o \frac{\partial^2 E_y}{\partial x^2} + B^o \frac{\partial^4 E_y}{\partial x^4} + C^o \frac{\partial^2 E_y}{\partial z^2} + D^o \frac{\partial^2 E_y}{\partial t^2} + \Gamma_1 |E_y|^2 E_y = 0 \qquad (8)$$

where the zero superscript indicates $n=n_o$ in ω_p^2 as follows;

$$A^o = A|_{n=n_o}, \text{ etc.} \qquad (9)$$

and where

$$\Gamma_1 = \frac{\left[\omega^2 (1 - D^o) + k_x^4 B^o - k_z^2 C^o\right] \left(\frac{\omega - \Omega'}{\omega}\right)}{\left(\frac{\omega - \Omega'}{k_x}\right)^2 - \frac{k_z^2}{k_x^2} v_z^2} \qquad (10)$$

The above technique is the same as that used in the previous nonlinear theory.

2.4 MULTIPLE TIME SCALING

Solving the full nonlinear partial differential equation is a formidable task. Yet, using a perturbation technique based on expansions in small amplitudes around an equilibrium value only restricts the problem requiring one to first linearize (8). Linearizing (8) would negate all the effort in getting (8) in the first place. Therefore, instead of using a perturbation technique based on expansions in small amplitudes, a technique based on expansions in time scales is used. This is the multiple time scales perturbation technique. (Nayfeh, 1973).

In the previous nonlinear theory (Thomas, 1981), the following ordering of partial derivatives was used;

$$\frac{\partial}{\partial t} = -i\omega - \delta u_c \frac{\partial}{\partial x'} + \delta^2 \frac{\partial}{\partial t'} \tag{11a}$$

$$\frac{\partial}{\partial x} = ik_x + \delta \frac{\partial}{\partial x'} \tag{11b}$$

$$\frac{\partial}{\partial y} = \delta^2 \frac{\partial}{\partial y'} \tag{11c}$$

$$\frac{\partial}{\partial z} = \delta \frac{\partial}{\partial z'} \tag{11d}$$

where δ is a small parameter indicating the order of time variations. In other words, higher powers of δ indicate more slowly varying quantities. It should be noted that a traveling wave solution is assumed. Variations in the $\hat{y}$ direction (see Figure 1) are considered second order since the $\hat{y}$ direction is neither the direction of propagation ($\hat{x}$ direction), the direction of bunching ($\hat{x}$ direction), or the direction of velocity drift (the $\hat{z}$ direction). Notice that the $\hat{z}$ direction is considered first order because the electrons

drift in this direction. Wave propagation along the $\hat{z}$ axis was neglected. Neglecting wave propagation along the $\hat{z}$ axis is thought to be a weak assumption; therefore, wave propagation is included in the analysis by including ik_z in (11d). Assuming that ik_z is a zero order (fast time scale) effect, (11d) becomes;

$$\frac{\partial}{\partial z} = ik_z + \delta \frac{\partial}{\partial z'} \tag{11d}$$

Substituting the expressions for the partial derivatives given in (11a)-(11d) into the nonlinear partial differential equation, (8), one obtains the following set of equations:

$$\underline{\delta}^0 \quad -A^0 k_x^2 - C^0 k_z^2 - D^0 \omega^2 = 0 \tag{12}$$

which yields the phase velocity (v_{pz}),

$$v_{pz} = \sqrt{\frac{-A^0}{D^0} \frac{k_x^2}{k_z^2} - \frac{C^0}{D^0}} \tag{13}$$

$$\underline{\delta}^1 \quad 2i\omega u_c D^0 \frac{\partial}{\partial x'} + 2ik_x A^0 \frac{\partial}{\partial x'} - 4ik_x^3 B^0 \frac{\partial}{\partial x'} + 2ik_z C^0 \frac{\partial}{\partial z'} = 0 \tag{14}$$

which yields the group velocity (u_c),

$$u_c = \frac{\omega}{k_x} + \frac{2k_x^3 B^0}{\omega D^0} + \left[\frac{C^0}{D^0} \frac{k_z^2}{\omega k_x} - \frac{C^0}{D^0} \frac{k_z}{\omega} \frac{\partial x'}{\partial z'} \right] \tag{15}$$

$$\underline{\delta}^2 \quad -2i\omega D^0 \frac{\partial}{\partial t'} - 2k_x^2 B^0 \frac{\partial^2}{\partial x'^2} + C^0 \left[\frac{\partial}{\partial z'^2} - \frac{k_z}{k_x} \frac{\partial^2}{\partial x' \partial z'} \right] = 0 \tag{16}$$

This second order equation models a slowly varying modulating envelope. The cubic nonlinear term is also considered second order resulting in the full nonlinear equation as follows;

$$-2i\omega D^{o} \frac{\partial E_y}{\partial t'} - 2k_x^2 B^{o} \frac{\partial^2 E_y}{\partial x'^2} + C^{o}\left[\frac{\partial^2 E_y}{\partial z'^2} - \frac{k_z}{k_x} \frac{\partial^2 E_y}{\partial x' \partial z'}\right] \tag{17}$$

$$+ \Gamma_1 |E_y|^2 E_y = 0$$

This equation is a modified form of the nonlinear Schrodinger equation (MNLSE) with a cubic nonlinearity. It is clear that keeping wave propagation in the $\hat{z}$ direction results in the additional term $-(k_z/k_x)(\partial^2 E_y/\partial x' \partial z')$. If $k_z=0$, the above nonlinear partial differential reduces to the equation derived in previous work. This additional term is the fourth major difference between the previous nonlinear theory and that presented here.

2.5 ORDERING THE TERMS OF THE MNLSE

Unfortunately, at this time it is not possible to solve analytically the MNLSE, (17), because of the additional spatial variation and because of the dependence of the coefficients on the rf electric field. Therefore, it is necessary to treat the additional terms, etc., as perturbations and obtain an ordering as follows;

zero order ϵ^{o}

$$-2i\omega D^{o} (E_y = \text{const}) \frac{\partial E_y}{\partial t} - 2k_x^2 B^{o} (E_y = \text{const}) \frac{\partial^2 E_y}{\partial x^2} \tag{18}$$

$$+ \Gamma_1 (E_y = \text{const}) |E_y|^2 E_y = 0$$

By setting B_y in the coefficients equal to a nonzero constant, the time varying nature of the coefficients is eliminated. When B^o is negative and Γ_1 is positive, (18) becomes the cubic nonlinear Schrodinger equation,

$$-i \frac{\partial E_y}{\partial t} + \frac{\partial^2 E_y}{\partial x^2} + |E_y|^2 E_y = 0 \tag{19}$$

which has stable (nonlinearly stable) soliton solutions.

first order ϵ^1

$$C^o \ (E_y = \text{const}) \left[\frac{\partial^2 E_y}{\partial z^2} - \frac{k_z}{k_x} \frac{\partial^2 E_y}{\partial x \partial z} \right] \tag{20}$$

The C^o term is considered a first order perturbation to the zero order solution. Higher order effects are those that result from E_y not equal to a constant, but where B_y in the coefficients is a function of time.

2.6 EFFECTS OF THE PERTURBATION TERMS ON THE NLSE

It is important to determine the effect that the additional term (the C^o term) has on the soliton solutions. Following Albowitz and Segur, 1979, the MNLSE is normalized to the following form;

$$iA_\tau + \lambda A_{\xi\xi} + \mu A_{\eta\eta} + \lambda |A|^2 A = 0 \tag{21}$$

where $\mu A_{\eta\eta}$ is the perturbing term.

From Albowitz and Segur, 1979, the following results are obtained;

a. CASE 1 $\mu > 0, \lambda > 0$

$$iA_\tau + A_{\xi\xi} + A_{\eta\eta} + |A|^2 A = 0 \tag{22}$$

This equation is unstable to symmetric perturbations (i.e., even mode) in the ξ direction.

b. CASE 2 $\mu>0$, $\lambda<0$

$$-iA_\tau+A_{\xi\xi}-A_{\eta\eta}+|A|^2A=0 \tag{23}$$

This equation is unstable to anti-symmetric perturbations (i.e., odd mode) in the ξ direction.

c. CASE 3 $\mu< 0$, $\lambda> 0$

$$iA_\tau+A_{\xi\xi}-A_{\eta\eta}+|A|^2A=0 \tag{24}$$

This equation is unstable to anti-symmetric perturbations in the ξ direction.

d. CASE 4 $\mu<0$, $\lambda<0$

$$-iA_\tau+A_{\xi\xi}+A_{\eta\eta}+|A|^2A=0 \tag{25}$$

This equation is unstable to symmetric perturbations in ξ.

To summarize the above cases, the additional spatial varying term results in the nonlinear instability of the soliton solution. The type of perturbation (symmetric or anti-symmetric) that results in the instability depends on the sign of the additional term. In a gyro-device, the nature of this nonlinear instability is related to the bunching of the electrons which cause the perturbation in the ξ direction. Depending on the signs of the coefficients, electron bunching around the zero of the rf field (anti-symmetric) or bunching around the maximum (symmetric) of the rf field will cause the nonlinear instability.

2.7 PARAMETER RANGE FOR GROWING SOLITON-LIKE SOLUTIONS

The final step in the general technique of modeling the dynamic nonlinear interaction in a gyro-device is to determine the region in parameter space where one expects growing soliton-like solutions to the MNLSE. In order to determine which of the possible forms (22)-(25) of the equation is the one of interest, the spatial location of the bunched electrons must be considered. Recall from section 2.2 that the ponderomotive force acting in the direction of rotation is responsible for electron bunching. The ponderomotive force causes bunching about the rf electric field zero which is an anti-symmetric perturbation. Consequently, only cases 2 and 3, (23) and (24) remain. The difference between these two cases is that (23) represents a system where the envelope group velocity is less than the wave phase velocity (see (15)) and (24) represents a system where the envelope group velocity is greater than the wave phase velocity. In the case of the gyro-device, the velocity of the bunched electrons is less than the wave phase velocity (in the $\hat{x}$ direction, not in the $\hat{z}$ direction), so (23) applies. To obtain (23) from (17), the coefficients must have the following signs;

D^o Positive

B^o Negative

C^o Negative

Γ_1 Positive

The range of d.c. magnetic field values over which growing soliton solutions are obtained is determined by considering the magnetic field values where the signs of the coefficients change from those listed above. First, consider the B^o coefficient. From

(4b), B^o is negative for $\omega<(k_{\parallel}v_{\parallel}+3\Omega)/\gamma-k_x E_y/B_o$. The regime of interest is where ω is near Ω, so the B^o is always negative. Next, consider the C^o coefficient. For the C^o term (4c) to be negative the following is obtained;

$$\left[\omega - (k_{\parallel}v_{\parallel} + \Omega)/\gamma - k_x E_y/B_o\right]^2 > \frac{-\omega_p^2 v_{\perp}^2}{c^2\gamma^2} \tag{26}$$

(26) is always true in the parameter regime of interest. For the complete C^o term to be negative

$$\frac{\partial^2 E_y}{\partial z^2} > \frac{k_z}{k_x}\frac{\partial^2 E_y}{\partial x \partial z} \tag{27}$$

must be true. From (27), the following constraint is obtained;

$$\frac{k_z}{k_x} < \frac{\partial E_y}{\partial z} \Big/ \frac{\partial E_y}{\partial x} \quad . \tag{28}$$

In other words, for large values of k_z, the variation of the field in the $\hat{x}$ direction must be small or the variation of the field in the $\hat{z}$ direction must be large. As expected, for positive wave numbers (forward wave interactions), the slope of the rf field is such that the rf field strength increases along the $\hat{z}$ direction. Consider the D^o coefficient. From (4d), D^o is positive when

$$\Omega < \gamma\omega \left[1 - \frac{\frac{\omega_p^2}{\gamma\omega^2}\frac{v_{\perp}^2}{2c^2\gamma^2}}{1 - \omega_p^2/\gamma\omega^2}\right]^{-1} - k_{\parallel}v_{\parallel} \tag{29}$$

with E_y assumed equal to zero. (29) provides the constraint on the maximum allowable

magnetic field for soliton solutions. The Γ_1 coefficient provides the lower magnetic field constraint. Notice from (10) that the Γ_1 behavior is dominated by the $1-D_o$ term. Therefore, Γ_1 is positive when

$$\Omega > \gamma\omega \left[1 + \frac{v_\perp^2}{2c^2\gamma^2} \right]^{-1} - k_\parallel v_\parallel \tag{30}$$

where E_y was assumed equal to zero. Of course, for the case where $E_y = 0$ the simple analytic solutions given in (29) and (30) are not complete. However, these equations illustrate the general characteristics of the operating regime of the gyro-device. The complete characteristics of the operating regime are given in the next section which discusses the saturation mechanism of the gyro-device interaction.

3.0 THE SATURATION MECHANISM

The saturation a of gyro-device occurs where the electrons have given up sufficient energy so that soliton solutions to the nonlinear partial differential equation are no longer possible. In other words, the maximum magnetic field value for electrons which have lost perpendicular energy to the wave ($B_H(E_y = 0)|_{v_{\perp f}}$) is less than the minimum magnetic field value for electrons which have not lost any perpendicular energy ($B_L(E_y = 0)|_{v_\perp}$). Therefore, full saturation occurs when,

$$B_L(E_y = 0)|_{v_\perp} = B_H(E_y = 0)|_{v_{\perp f}}. \tag{31}$$

The constraint in (31) allows the perpendicular electron energy to decrease smoothly from the initial value to the final value without interruption. In other words, growing soliton solutions are possible over the full range of $v_\perp$ values given a proper value for the rf electric field.

It is important to include rf field effects so that both the magnetic field for peak output power (B_p) and the actual value of the output power at B_p can be determined. The rf electric field (E_y) results in a change in rotational electron velocity through an $E_y \times B_o$ drift. Clearly, the electrons are accelerated or decelerated depending on the sign of the rf field. The sign of the rf field depends upon the location of the electron in its orbit. Maximum output power is achieved when the maximum number of electrons are located in a favorable position in the rf field. The favorable position in the rf field is defined as the spatial location or locations where conditions are such that soliton solutions exist to the nonlinear partial differential equation. Clearly, maximum output power would be obtained if the entire electron orbit constitutes a favorable position. This would occur if an electron in either the positive or negative rf field can contribute to the growth of the rf field. Therefore, the following expression is obtained;

$$B_H(E_y+)\big|_{v_\perp - \Delta v_\perp} = B_H(E_y-)\big|_{v_{\perp f} - \Delta v_\perp} \tag{32}$$

The value of magnetic field that satisfies (32) is the optimum B_p for the particular design under consideration. The $\Delta v_\perp$ term takes into account the effect of the $E_{rf} \times B_o$ drift on the rotational velocity of the electrons.

Notice that $\Delta v_\perp$ is subtracted from both $v_\perp$ and $v_{\perp f}$ and not subtracted from $v_\perp$ and added to $v_{\perp f}$ as one would suspect from the sign of E_y shown in (32). The reason that $-\Delta v_\perp$ is used is that $v_{\perp f} - \Delta v_\perp$ is the minimum perpendicular velocity possible from the interaction and describes electrons which have lost the most perpendicular energy. These electrons are bunched at the location in the electron orbit where the rf field is directed perpendicular to the motion of the electron, (Figure 3).

Having obtained the optimum B_p and the maximum perpendicular energy lost to the rf wave, the rest of the operating characteristics can be determined. First, the

efficiency is found from the following;

$$\eta = \frac{(\gamma_{INITIAL} - 1) - (\gamma_{FINAL} - 1)}{(\gamma_{INITIAL} - 1)} \tag{33}$$

where $v_\perp$ is used to obtain $\gamma_{INITIAL}$ and $v_{\perp f} - \Delta v_\perp$ is used to obtain γ_{FINAL}. The rf electric field strength is determined from $\Delta v_\perp$ as follows;

$$E_{rf} = \Delta v_\perp B_o \tag{34}$$

The rf electric field strength is converted to rf output power by considering an interaction impedance. For a gyrotron (i.e., a cavity structure),

$$P_c = \frac{|E|^2}{QK_L} \tag{35}$$

where P_c is power in the cavity, Q is the loaded Q, E is the rf field strength, and K_L is related to the interaction impedance. One need only to determine K_L for the particular cavity in question. With the power, efficiency, and d.c. voltage (which determines the value for $v_\parallel$), the optimum operating current is obtained from

$$I = P_c/\eta V_A. \tag{36}$$

In summary, the following optimum operating point characteristics of a particular design can be obtained from the nonlinear theory;

d.c. magnetic field

rf field strength

rf output power

efficiency

current

where the input parameters are the frequency, the d.c. voltage, $v_\perp$, v_w, and the parallel and perpendicular wave numbers. The only additional parameters necessary are those to convert rf field strength to output power.

4.0 COMPARISONS

4.1 COMPARISON OF NONLINEAR THEORY AND COMPUTER SIMULATIONS

In order to verify that the nonlinear theory is correct, a comparison is made between the optimum operating characteristics for a particular design as predicted by the nonlinear theory versus those obtained from a computer simulation. The particular design used for this comparison is as follows;

$$f_o = 60 \text{ GHz}$$

$$k_w = 1.013 \text{ cm}^{-1}$$

$$k_\perp = 11.14 \text{ cm}^{-1}$$

$$v_w = 0.225 \text{ c}$$

$$v_\perp = 0.45 \text{ c}$$

$$V_a = 80.0 \text{ kV}$$

With (31) through (36), the following are obtained from the nonlinear theory;

$$B_p = 23.02 \text{ kG}$$

$$E_{rf} = 2.43 \times 10^7 \text{ V/m}$$

$$P_c = 324 \text{ kW}$$

$$\eta = 58.67\%$$

$$I = 6.9 \text{ A}$$

$$v_{\perp 0} = 0.294c$$

$$\Delta v_\perp = 0.034c$$

The loaded Q for this particular design is 400 and K_L which is determined from a Varian computer code that solves the eigenvalue problem for the cavity is 4.545×10^9 yielding P_c = 324 kW for $E_{rf} = 2.43 \times 10^7$ V/m.

The results from the computer simulation for the above design are shown in Figure 4, (Shively, et. al., 1982). The computer code that was used is a two dimensional, fully relativistic, large signal code developed at Varian Microwave Tube Division that includes both E_{rf} and B_{rf} with no averaging over a gyroradius where the effects of the electron beam on cavity Q and the rf field profile are not included. In Figure 5, the point in parameter space obtained from the theory is shown with the results of the computer simulation. Consider the following: First, the theoretical value of efficiency at 6.9A lies very close to the value obtained with the computer simulation; second, even though the theoretical optimum point in parameter space is higher in current than the optimum point from the computer simulation, (i.e., 6.9A versus 5.7A), this discrepancy is most likely a result of incomplete simulation results. The most information obtained from Figure 4 is that the optimum operating point is where the magnetic field is between 22.93 kG and 23.05 kG and the current is between 5.7A and 8.8A. Clearly, the optimum point is closest to 23.05 kG and 5.7A. It is possible that the optimum operating point is the same as the theoretical value--23.02 kG and 6.9A. In Figure 5, the dashed line indicates a possible simulation curve for a magnetic field of 23.02 kG. Such a curve indicates that the nonlinear theory accurately predicts the optimum operating point for a particular gyro-device design.

In addition to comparing the theoretical and computer results for the optimum operating point, it is useful to make comparisons at other values of magnetic field and current. Theoretical predictions are obtained from (32) by substituting various values of $v_\perp'$ for $v_{\perp f} - \alpha v_\perp$ where $v_\perp' > v_{\perp f}$. The theoretical values for $v_\perp' = 0.325c$ and $0.294c$ are 23.34 kG, 5.08A and 23.18 kG, 6.175A, respectively. These values are compared to the

computer results in Figure 6 demonstrating close agreement. From the nonlinear theory, the line shown in Figure 6 is generated with the endpoint being the optimum operating point.

4.2 COMPARISON OF THE NONLINEAR THEORY AND EXPERIMENTAL DATA

Having shown close agreement between predictions of the nonlinear theory and results of the computer simulations, a comparison is made between predictions of the nonlinear theory and available experimental data. The experimental data (Figure 7) were obtained from a Varian 60 GHz gyrotron operating under pulsed conditions. From Figure 7 (Felch, et. al., 1982), the following experimental values are obtained;

I(AMPS)	B_p^E	f_o(GHz)	η^E(%)	P^E(kW)	B_H^E(kG)
4.0	23.30	59.68	23.5	75	24.0
6.0	23.17	59.67	27.2	135	24.1
8.1	23.07	59.67	32.5	210	24.2

The values of $v_\perp$ for the various currents are obtained from the following;

$$B_H^E = B_H \ (E_y = 0) \ |v_\perp \tag{37}$$

Assuming that the values of B_p^E given in the preceding table satisfy (32) and using the values of $v_\perp$ obtained from (37), E_{if} and $v_{\perp f}$ are determined. With the cavity's K_L obtained from a Varian computer code, the rf field is converted to power. The efficiency is obtained by substituting $v_{\perp f}$ and $v_\perp$ into (33). The complete results from the theory are summarized below;

I(AMPS)	$v_\perp$	P^T(kW)	η^T(%)
4.0	0.420c	70.9	30.75
6.0	0.432c	160.1	43.60
8.1	0.440c	234.5	51.49

Comparing the theoretical results with the experimental data, a number of points can be made. First, considering the gun design, the values of $\alpha(\alpha=v_\perp/v_\parallel)$ are reasonable (i.e., $1.87<\alpha<1.96$). Second, the power predicted by the theory is well within 20% of the experimental values. Third, the theoretical efficiency is significantly higher than the experimental values, but the computer simulation results are no better. Of course, both the nonlinear theory and the computer simulation assume no velocity spread in the electron beam. It is likely that velocity spread effects, as well as effects due to the fact that all the electrons are not located at the electric field maximum of the TE_{02} mode account for the lower efficiencies seen in the experimental data. In light of these caveats, one can conclude that there is reasonable agreement between the nonlinear theory and the experimental data.

5.0 CONCLUSION

It has been shown that the soliton-based nonlinear gyro-device theory allows one to predict the optimum operating point for a particular design. The optimum current, magnetic field, efficiency, and power are obtained. Comparisons of the theoretical predictions to computer simulation work done at Varian's Microwave Tube Division show close agreement not only for the optimum operating point, but for other points in parameter space as well. Comparisons of the theory with Varian 60 GHz gyrotron data show reasonable agreement when the effects of velocity spread and electrons off the B field maximum are considered.

Having demonstrated that the nonlinear theory agrees with simulation and experiment, work can begin on understanding the full effect of the nonlinearity. Some areas of immediate interest are harmonic generation and modulational effects (i.e., amplitude, frequency, and phase).

References

Albowitz, M., and Segur, H., 1979, J. Fluid Mech. 92 (4), 691.

Chu, K. R., Drobot, A.T., Granatstein, V. L., and Seftor, J. L., 1979, I.E.E.E. Trans. Microw. Theory Tech. 27, 178.

Felch, K., Evans, S., Fox, L., Jory, H., Shively, J., Spang, S., 1982, I.E.E.E. Int. Conf. Plasma Science, Ottawa, Conf. Digest, 45.

Flyagin, V.A., Gaponov, A.V., Petelin, M.I., and Yulpatov, V. K., I.E.E.E. Trans. Microw. Theory Tech 25, 514.

Krall, N., and Trivelpiece, A., 1973, Principles of Plasma Physics, (New York: McGraw-Hill).

Nayfeh, A., 1973, Perturbation Methods, (New York: Wiley).

Shively, J., et. al., 1982, Quarterly Report No. 13, 60 GHz Gyrotron Development Program Prepared by Varian Associates, Inc. under Subcontract P. O. No. 534-21453C for ORNL operated by Union Carbide Corp. for U. S. DOE under contract W-7405-ENG-26.

Thomas, G. E., 1981, Int. J. Electronics, 51 (4), 395; 1983, Int. Conf. Infrared and Mmwaves, Miami Beach, Conf. Digest.

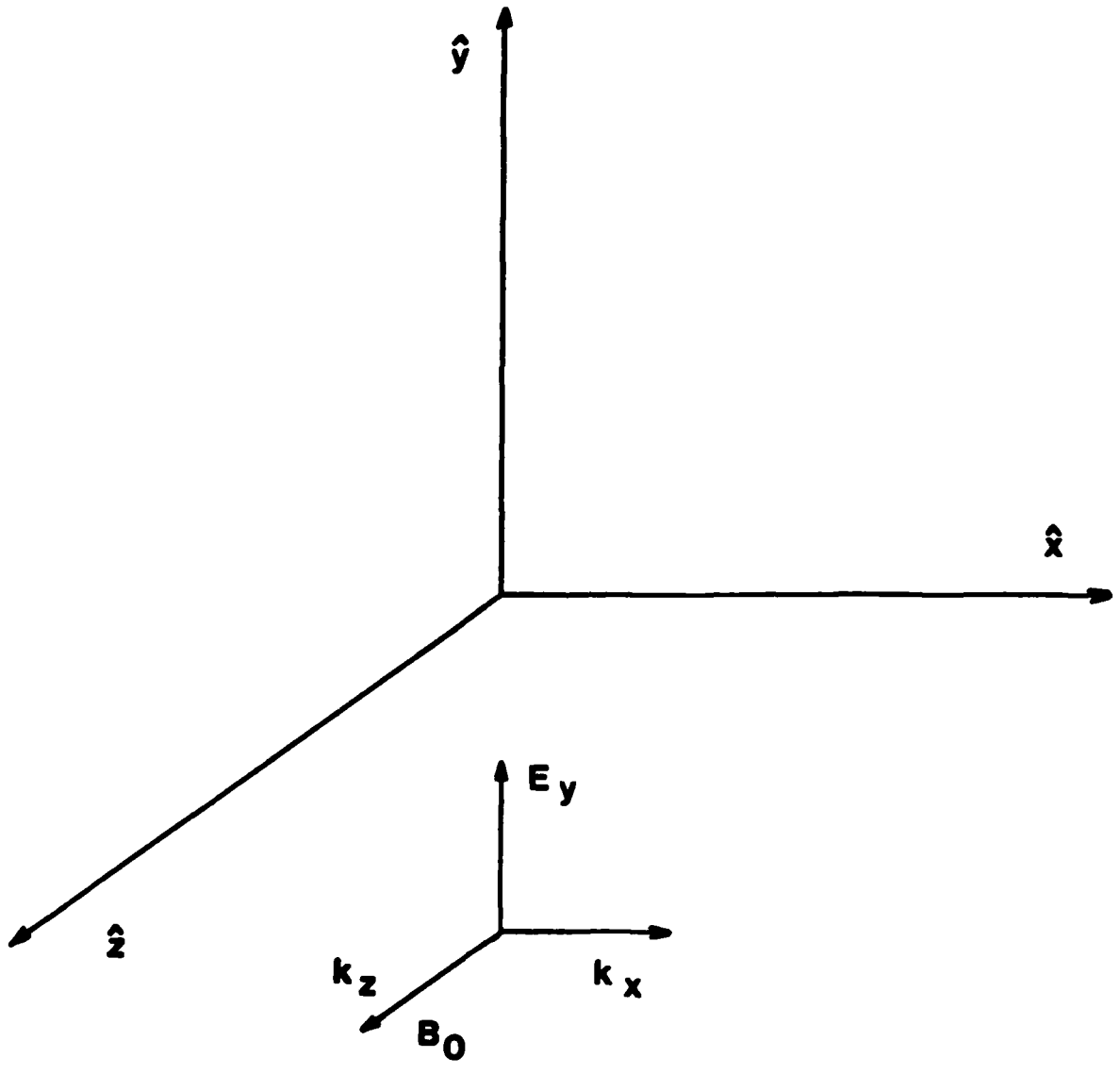

FIGURE 1 GYRO DEVICE GEOMETRY

(FLYAGIN, ET. AL., 1977)

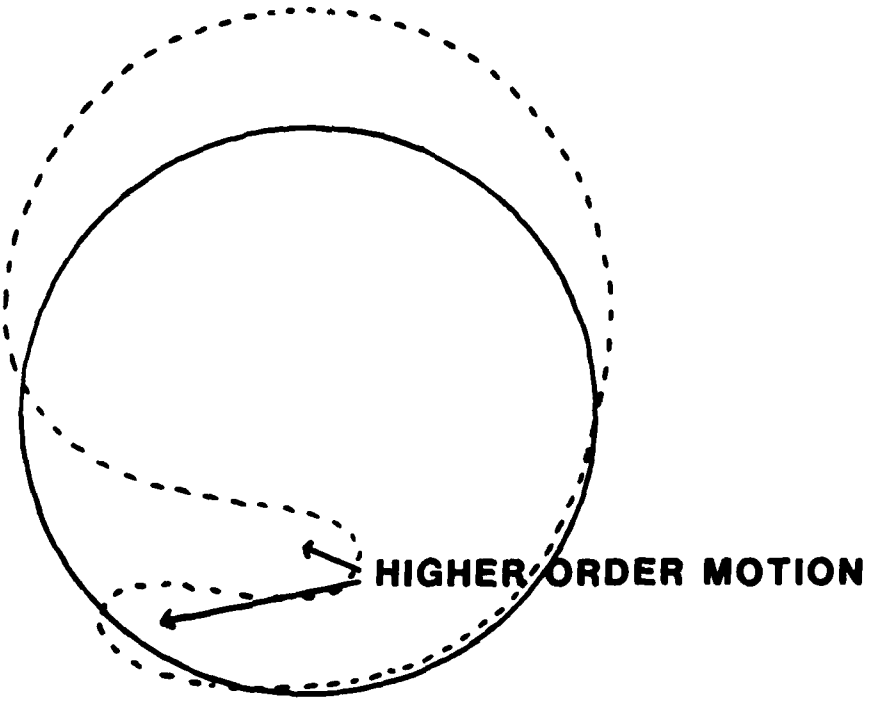

FIGURE 2 HIGHER ORDER ELECTRON MOTION

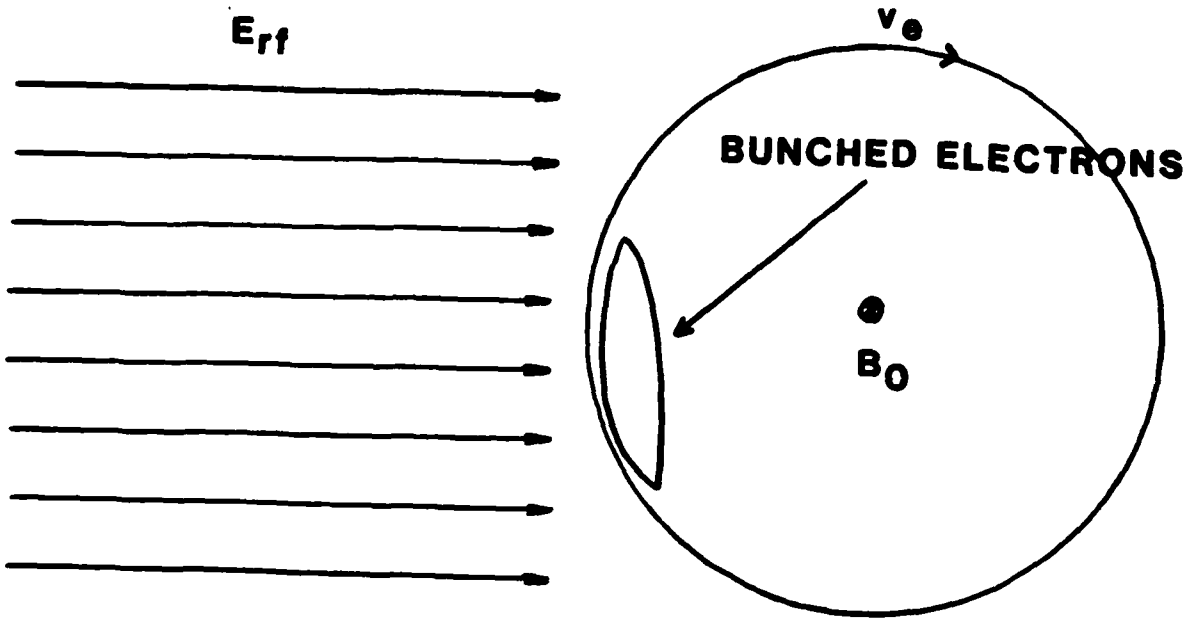

FIGURE 3 LOCATION OF BUNCHED ELECTRONS

FROM (SHIVELY, ET. AL., 1982)

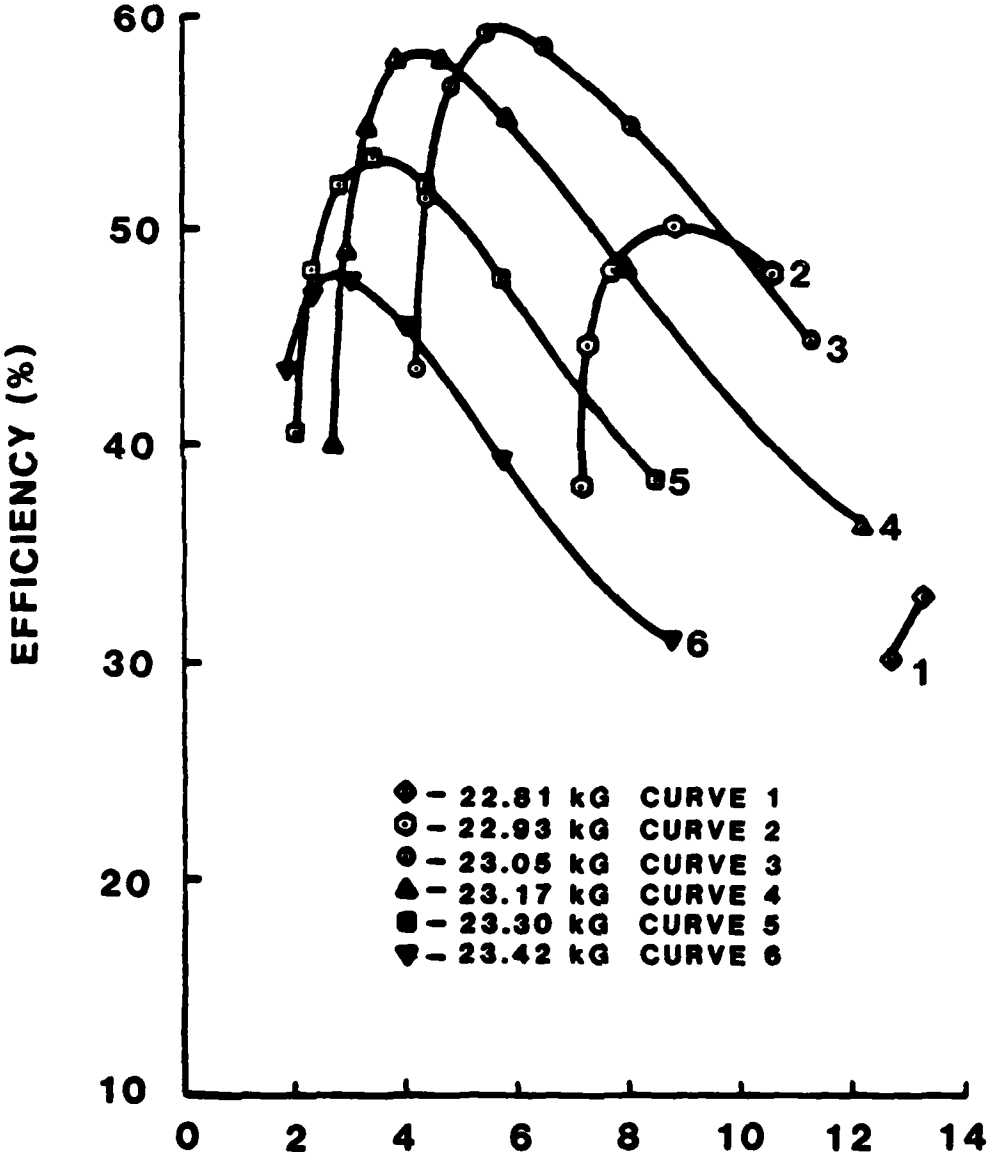

FIGURE 4

FROM (SHIVELY, ET. AL., 1982)

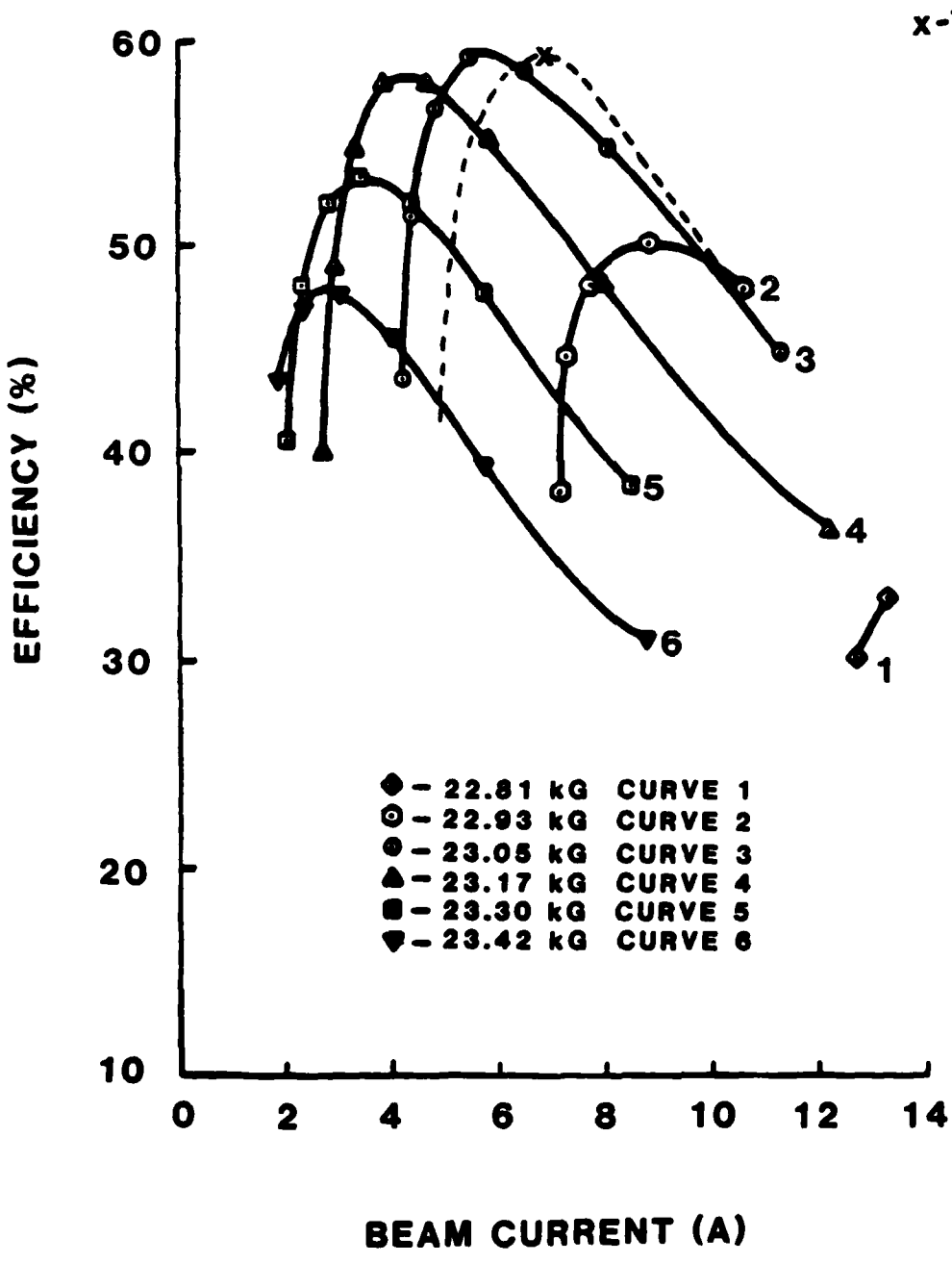

FIGURE 5

FROM (SHIVELY, ET. AL., 1982)

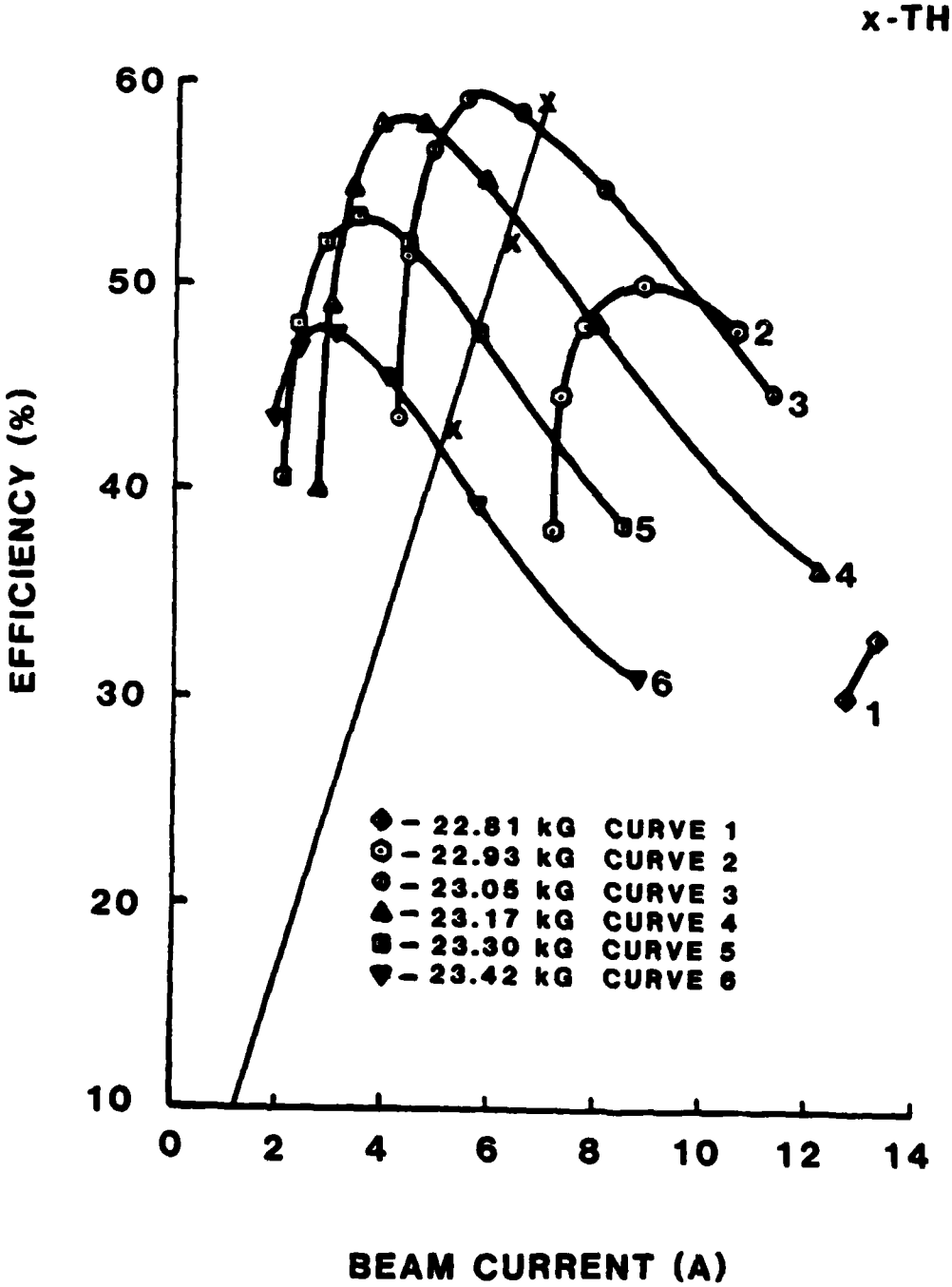

FIGURE 6

VGE-8060 S/N X-3R
OUTPUT POWER FOR
VARIOUS BEAM CURRENTS

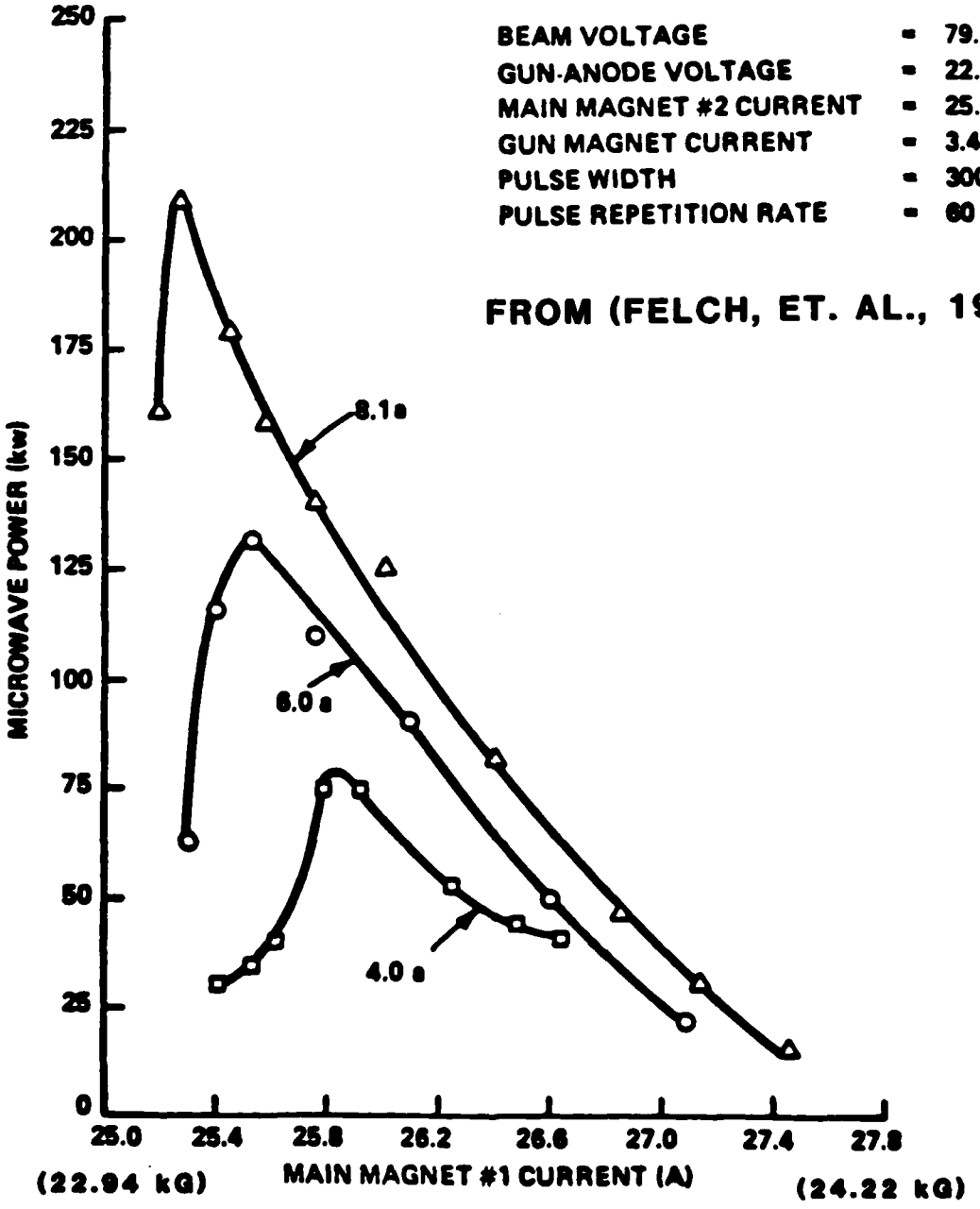

FIGURE 7